JOURNAL OF MECHANICAL ENGINEERING AND SCIENCES
ISSN: 2289-4659 e-ISSN: 2231-8380
VOLUME 19, ISSUE 4, 2025, 10898 - 10907
DOI: https://doi.org/10.15282/jmes.19.4.2025.6.0854

RESEARCH ARTICLE

Investigation of the structural deformations of various plastic spoilers with NACA 6409 cross section at subcritical Reynolds Numbers under different angles of attack

Luigi Buffone[1]*, Georgios Manganos[2], Kavitha Mol S[3]

[1] School of Automotive Engineering, Wuhan University of Technology (WUT), 122 Luoshi Road, Wuhan 430070, Hubei, China
[2] Faculty of Engineering Mechanics, Slovak University of Technology in Bratislava (STU), Nám. slobody 17, 812 31 Bratislava, Slovakia
[3] Department of Mechanical Engineering, Government Polytechnic College, Ezhukone, Kerala 691505, India

ABSTRACT - This study investigates the aerodynamic performance and structural deformations of finite rectangular planform wings with a spoiler with a NACA 6409 airfoil section, fabricated from 3D-printed plastic materials. Unlike conventional aluminum or carbon fiber spoilers, plastic components with a high aspect ratio exhibit more pronounced aeroelastic effects, making their characterization important for practical applications. The main objective was to evaluate aerodynamic loads and resulting deformations through both experimental wind tunnel testing and numerical simulations. Wings with dimensions of 100 × 400 mm were fabricated using additive manufacturing techniques (MJF and SLS) with Nylon PA12, Resin CUV9400, and Nylon PA12GB materials. Tests were conducted at uniform wind speeds up to 30 m/s and varying angles of attack. Results show that the maximum Y displacement occurred at 10° and 30 m/s, with values of –51.03 mm for Nylon PA12, –26.52 mm for Resin CUV9400, and –21.73 mm for Nylon PA12GB. The maximum von Mises stress reached 10.7 MPa, 10.9 MPa, and 11 MPa for the three materials, respectively. Numerical simulations showed close agreement with experiments, with deviations below 6% for deflection and 4.37% for torsion. In conclusion, Nylon PA12GB demonstrated superior performance due to its lower deformation, confirming its suitability for cost-effective and lightweight aerodynamic applications.

ARTICLE HISTORY
Received : 06th Jun. 2025
Revised : 28th Oct. 2025
Accepted : 05th Nov. 2025
Published : 29th Dec. 2025

KEYWORDS
Fluid structure interaction
Rear spoiler
Wind tunnel test

1. INTRODUCTION

A spoiler functions as an inverted wing that generates downforce with a high lift-to-drag ratio [1], a key factor for improving traction and stability during cornering [2]. Its effectiveness depends primarily on the ability to produce sufficient downward aerodynamic forces [3], which not only enhance vehicle stability but also reduce the airflow beneath the vehicle, thereby lowering fuel consumption [4]. The aerodynamic performance of spoilers has been extensively examined through both experimental and numerical methods [5]. To minimize material costs, alternatives such as fiberglass, carbon fiber, ABS plastic, and silicone have been investigated [6]. Compared to conventional materials, spoilers fabricated from synthetic and natural fibers are lighter and more economical, while additive manufacturing provides further opportunities for producing spoiler components using plastic-based materials. However, the mechanical flexibility of 3D-printed spoilers relative to conventional rigid designs requires further study [7]. In this study, the aerodynamic and structural behavior of a NACA 6409 spoiler was investigated using Multiphysics simulations in ANSYS, highlighting the efficiency and cost-effectiveness of numerical analyses for parametric studies. Experimental tests were performed selectively to validate the simulation results. Three 3D-printed materials—Nylon PA12 (PA12), Resin CUV9400 (CUV9400), and Nylon PA12GB (PA12GB)—were assessed to develop an economical and innovative spoiler design. The findings indicate promising potential for lightweight, recyclable, and cost-efficient spoiler solutions in automotive applications.

2. MATERIALS AND METHODS

The spoilers were evaluated through both numerical simulations and experimental testing. Finite Element Analysis (FEA) was conducted using software equipped with integrated modules: a CAD module for geometry generation, a CFD module for computing aerodynamic forces, and a FEM module for assessing both flexural and torsional deformations. In parallel, physical models were fabricated using MJF and SLS additive manufacturing technologies and tested in a wind tunnel to measure aerodynamic loads [8]. Sensors mounted on the models, connected to a data acquisition (DAQ) system, recorded deformation responses at varying velocities and angles of attack. Finally, the numerical predictions were systematically compared with the experimental measurements to identify and analyze discrepancies.

2.1 Theoretical Method

The fluid–structure interaction (FSI) of the spoiler was simulated using ANSYS software with a one-way coupling approach. In this framework, the CFD module computed the pressure distribution on the spoiler surfaces, while the FEM

*CORRESPONDING AUTHOR | Luigi Buffone | ✉ luigibuffone@yahoo.com

module evaluated the resulting structural deformations (Figure 1) [9,10]. Since the spoiler operates under low Reynolds number airflow, the structural elastic response needed to be captured accurately. The flow field was solved using the Reynolds-Averaged Navier–Stokes (RANS) equations along with the associated turbulence closure models [11]. The turbulence model used in this simulation was the SST k-ω with two equation model which involves solving two essential transport equations [12]. The choice of the turbulent SST (Shear-Stress Transport) k-ω model is justified for this simulation, as it involves a low-Reynolds-number external flow without heat exchange between the spoiler and the air. [13]. The dominant aerodynamic loads on the spoiler consist of bending and torsional forces, which induce deformations. Due to the significant tip displacement expected, the 'Large Deflection' (NLGEOM) setting was enabled to account for geometric nonlinearity, extending the analysis beyond simple linear Hooke's law approximations [14].

Lift is proportional to the square of the velocity. The lift force is proportional to the square of the air velocity and is given by:

$$L = 1/2\rho V^2 S C_L = qSC_L \quad (1)$$

where L is the lift force, ρ is the air density, v is the airspeed, q is the dynamic pressure $0.5\rho V^2$, S is the reference area, and C_L is the coefficient of lift. The coefficient of pitching moment is a dimensionless number that depends on factors such as the angle of attack [15].

The pitching moment about the Z-axis is proportional to the air velocity as well as the aerodynamic moments and is given below:

$$M = 1/2\rho V^2 S C_M = qSC_M \quad (2)$$

where M is the pitching moment, ρ is the air density, v is the airspeed, q is the dynamic pressure $0.5\rho V^2$, S is the reference area, and C_M is the coefficient of pitching. The coefficient of lift is a dimensionless number that depends on factors such as the angle of attack [16].

The spoiler chord length and span are 100 mm and 400 mm, respectively, with an aspect ratio of 4. The D-type fluid domain was created around the spoiler for numerical analysis, as shown in Figure 1a, with a semi-circular inlet to reduce domain volume [17]. A cylindrical subdomain was introduced around the spoiler to facilitate rotation and enable variable cell size mesh generation.

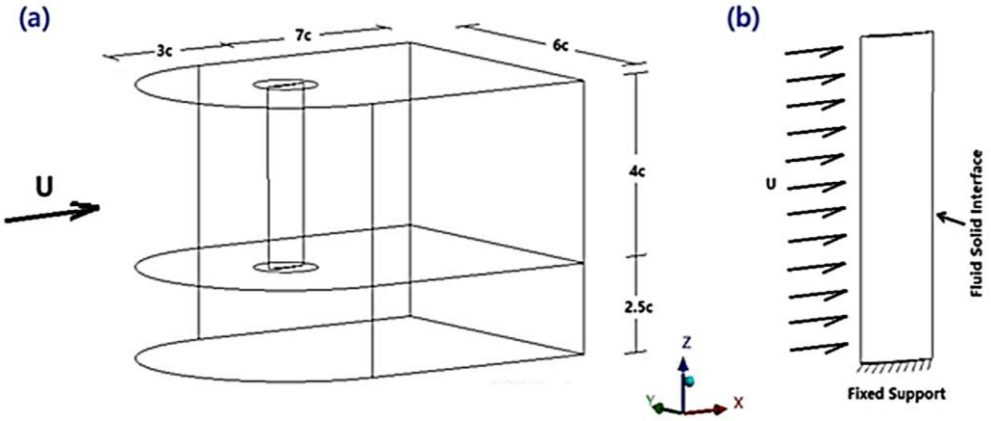

Figure 1. (a) Fluid Domain - (b) Structural Domain

Figure 1 illustrates the computational setup: (a) the fluid domain and (b) the structural domain. The fluid domain extends 3C upstream and 7C downstream from the spoiler's chord center, with lateral extensions of 3C on each side to minimize blockage effects. For the cantilever configuration, the spanwise domain extends 2.5C from the wing root (Figure 1a). The structural model represents a cantilever beam, with the lower portion fixed at the support and the upper portion free to deform (Figure 1b).

The study was parametric with two different types of parameters: fixed parameters and variable ones. The fixed parameters are the analysis type, which was set to steady flow; the outlet pressure, set to zero; and the turbulence model, set to SST k-ω [18]. The air velocity and angle of attack are the variable parameters. Specifically, the air velocity ranges from 10 to 30 m/s with a step of 5 m/s, and the angle of attack ranges from 0° to 20° with a step of 5° (Table 1). The mesh utilized in the fluid dynamics study comprises polyhedral cells, which combine the benefits of reduced distortion and enhanced solution convergence speed (see Figure 2) [19]. The independent mesh investigation was conducted in the layer perpendicular to the model's surface using the formula $\frac{0.1}{Re^{0.5}}$, (Re $=\frac{v*l}{\nu}$) where Re is the Reynolds number (198,531 in this case), v is the maximum velocity (30 m/s), l is the chord length of the spoiler (0.1 m), and ν is the kinematic viscosity of air (1.5111×10^{-11} for a temperature of 20 °C) [20].

Table 1. Various parameters of input and values

Fluid Domain	Value	Structural Domain	Value
Analysis Type	Steady Flow	Analysis Type	Steady Structure
Inlet Velocity [m/s]	10, 15, 20, 25, 30	Type of Load	Distribute Load
Angle of Attack [deg]	0, 5, 10, 15, 20	Angle of Attack [deg]	0, 5, 10, 15, 20
Outlet Pressure	0 Pa	Configuration	Cantilever Beam
Turbulent Model	SST k-ω	Support Type	Fixed
		Large Deflection	On

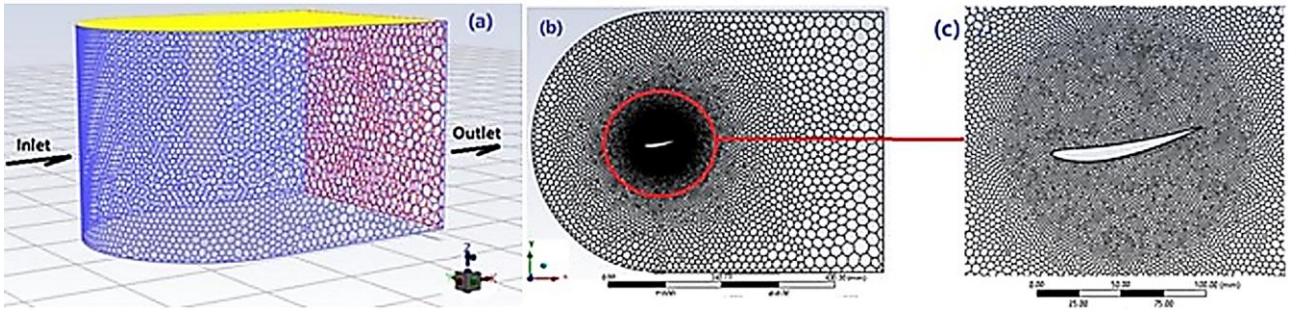

Figure 2. Case study problem mesh (a) Computational domain (b) Top view (c) Zoomed views

In order to find the independent meshes five Polyhedral geometries for CFD module and four Hexahedral geometries for FEM module were used. The most suitable mesh consisted of 2,165,238 nodes and 444,623 elements, featuring a minimum orthogonal quality of 0.307882 and a maximum aspect ratio of 14.2999 [21]. The most suitable mesh was made by length equal to 2.125 mm, an average aspect ratio of 1.5608, an average Jacobian of 0.88661 from the Gauss Point of view, and skewness factors ranging from a minimum of 2.1086 x 10^{-3} to a maximum of 0.13851 [22]. Two paths are considered for analyzing the spoiler deformations [23], with two sensors installed on them: Path A, subjected to only deflection, and Path B, subjected to both deflection and torsion, with a distance equal to 60% of the spoiler's chord (see Figure 1). According to the principle of superposition of effects, the formation at point B2 is the sum of the bending deformation and the torsional deformation [24].

$$\delta_{(f+t)} = \delta_f + \delta_t = \left(y_{(A2)}\right)/(4c) + \left(y_{(A2)} - y_{(B2)}\right)/(0.6c) \quad (3)$$

where $\delta_{f+t} = y_{B2}$is slope due to total deformation, $\delta_f = y_{A2}$is slope due to flexional deformation, $\delta_t$is slope due to torsional deformation, l=4c is spoiler span (see Figure 2b and 2c).

Considering the generic section (z) shown in the (zy) plane and analyzing the forces acting on the right side of the beam, the moment is equal to that reported in the second term of the elastic curve equation for bending and is:

$$EI\left(d^2 y_{(A2)}\right)/(dz^2) = M_f \quad (4)$$

where M_f is the bending moment obtained by the product of lift and half the length of the spoiler, which is qSC_L2c, and EI is the flexural rigidity of spoiler (see Figure 3) [25].

The torsion was calculated by considering the difference between path A and path B, and the point of maximum torsion is represented by the relative movement of point B2. The torsional angle that is the difference between y_{B2} and y_{A2} is generate from the torsional moment and is:

$$GJ(d\theta_z)/dz = M_t \quad (5)$$

where M_t is torsional moment along the Z-axis and it is the product between aerodynamic axis and elastic axis is the torsional moment having the same form of bending moment due to distribute force q substituted and reported in the second term of elastic equation for torsional moment (see Figure 3) [26].

Considering that the position of the spoiler in the wind tunnel is vertical, the force of gravity acts along the Z-axis, being zero along the Y-axis (see Figure 3). By integrating once and solving the equation, the constant C1,x can be determined at point were z=0 that is the elastic point where the torsion is equal to zero and corresponding to x=0. The equations presented are formulated in relation to the torsion and flexure of an isotropic beam, where GJ represents torsional rigidity, and EI represents flexural rigidity [27]. The application of the Euler–Bernoulli beam theory of the beam is evident, which is a structural theory used to analyze the response of a beam where loads are applied [28].

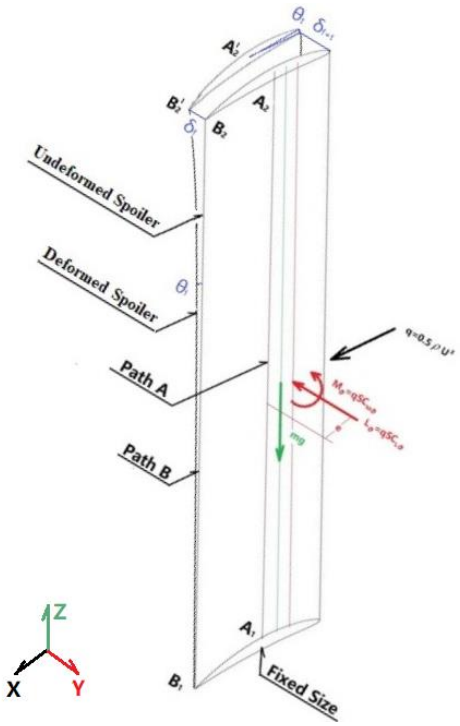

Figure 3. Undeformed and deformed spoiler with paths and aerodynamic forces

2.2 Experimental Method

The spoilers were fabricated using different materials—PA12, CUV9400, and PA12GB—to achieve cost efficiency and smooth aerodynamic surfaces [29]. The PA12 and PA12GB models were manufactured using HP's Multi Jet Fusion (MJF) technology. In this process, a thin layer of polymer powder enriched with additives is deposited on a build platform via a multi-jet system. An infrared source, activated by fusing and detailing agents, selectively sinters the powder to form the desired geometry, layer by layer [30,31]. In contrast, the CUV9400 model was produced using Selective Laser Sintering (SLS) technology. Here, a laser beam selectively fuses successive layers of polymer powder, building the component directly from the digital model with high precision [32,33].

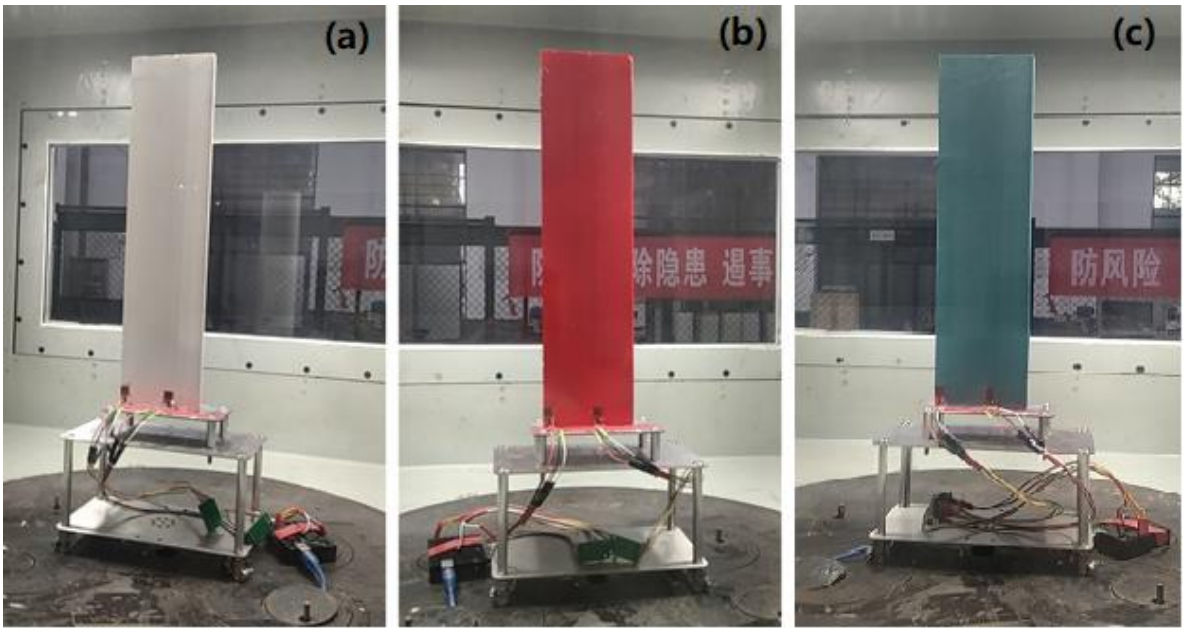

Figure 4. Different spoiler material in the test section of wind tunnel (a), PA12 (b), CUV9400 and (c) PA12GB

The experiments were carried out in an open-type subsonic wind tunnel at Wuhan University of Technology, with a maximum operating velocity of 40 m/s corresponding to a Mach number of 0.1156 [34]. The test section measured 2.0 × 1.2 × 0.8 m, within which the spoiler was mounted vertically (Figures 4a–4c). A rotating disk allowed variation of the angle of attack from −30° to +30° in precise increments. Aerodynamic loads were transmitted to a drag balance through a rigid support frame. Test conditions included wind speeds of 10, 20, and 30 m/s, and angles of attack ranging from 0° to 20° in steps of 5°.

Two data acquisition (DAQ) systems were employed. The wind tunnel's internal DAQ system recorded flow and aerodynamic force parameters, while an Arduino-based system captured structural deformation data. An Arduino UNO microcontroller (Figure 5a), programmed in Arduino IDE and operating at a sampling rate of 20 Hz, was used for this purpose [35,36]. Strain gauges were positioned 40 mm from the fixed support—one near the leading edge and the other close to the torsional axis (Figures 4a–4c) [37]—to measure maximum tensile stress. Calibration was performed to establish the relationship between strain and stress, converting the strain gauge's millivolt output into displacement [38]. To measure spoiler deflection, a calibration procedure was carried out using a concentrated load: a series of metallic discs, each weighing 113 g, were placed at the free end of the structure (Figure 5a). This allowed the strain gauge signals to be correlated with the vertical displacement δ of point A2 relative to point A1 (Figure 5a).

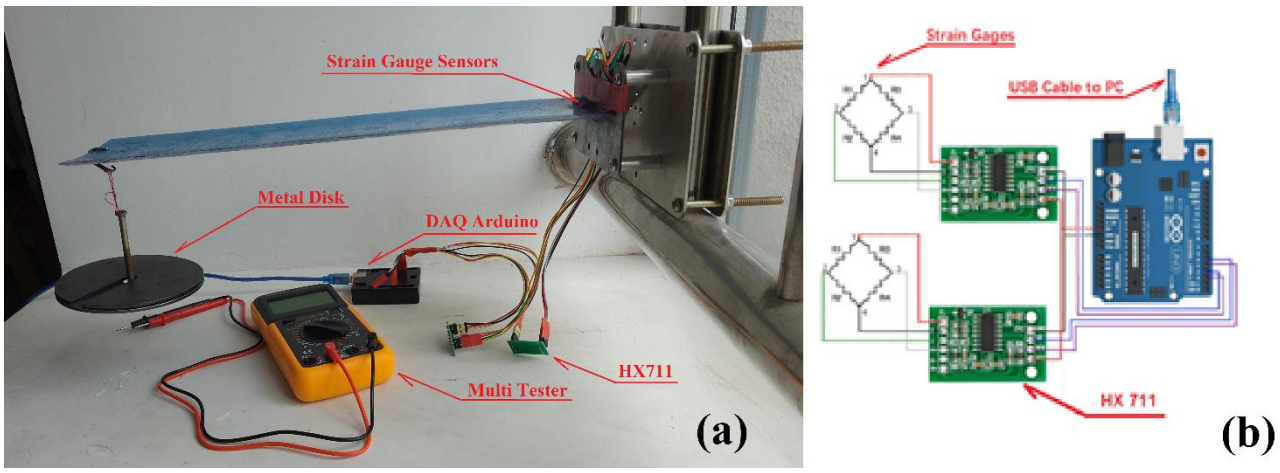

Figure 5. Spoiler deflection under load test Electric (a) Electric Scheme of DAQ (b) [27]

The vertical deflection of point A_2 which corresponds to δ, of the spoiler is obtained from the measured bending strains by solving the equation using the finite difference approximation method, where $sin\,\phi = dy_{A_2}/ds$ [39, 40].

$$\delta = \sqrt{((EI)/(2F))} \int \_0\text{^}(\phi\_0)\, (\sin\, \phi d\phi)/(\sqrt{(\sin\, \phi\_0 - \sin\, \phi)}) \quad (6)$$

where: $\delta = y_{A_2}$ is the vertical deflection of A_2 point, E is the modulus of elasticity, I is the moment of inertia of the cross-section of the spoiler, F is the external load applied to the A_2 point, ϕ_0 is the rotation angle of A_2 point and ϕ is the rotational angle of generic point between A_1 and A_2, and s is the generic portion of spoiler between A_1 and A_2.

$$\delta = \sqrt{\frac{EI}{2F}} \int_0^{\phi} \frac{sin\,\phi d\phi}{\sqrt{sin\,\phi_0 - sin\,\phi}} \quad (7)$$

3. RESULTS AND DISCUSSION

This study evaluates the flexural and torsional deformations of plastic spoilers subjected to distributed wind loads, offering important insights into their aerodynamic behavior. In the one-way FSI analysis, deformations of the High Aspect Ratio Spoiler (HARS) were measured, revealing that flexural deformations were substantially larger than torsional ones. The aerodynamic forces directly influenced both deformation modes, with plastic spoilers produced by 3D printing exhibiting high elastic flexibility. Unlike conventional spoilers made from aluminum or composite materials, which show minimal deformation, the plastic spoilers demonstrated significant yet non-critical elastic deformations that did not compromise structural integrity.

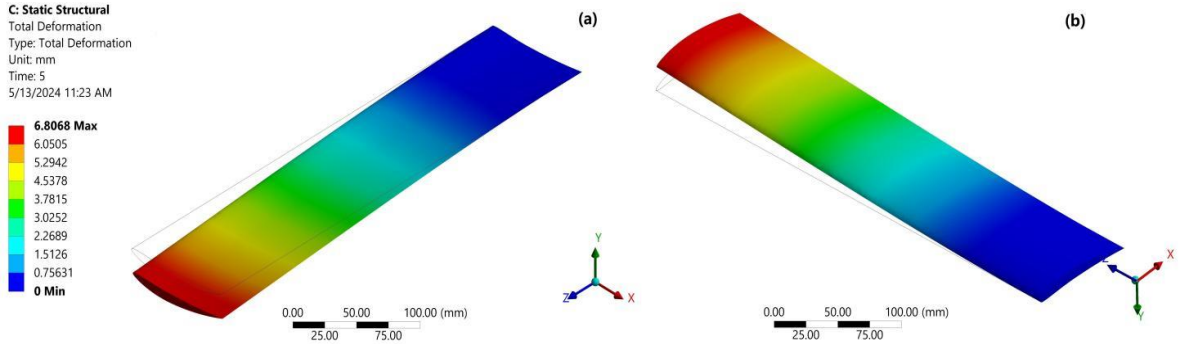

Figure 6. Spoiler total deformation maps of CUV9400 at AOA 0 deg and 20 m/s (a) Top (b) Bottom

The pressure distribution pattern was consistent across different spans, although the magnitude varied with span length. Specifically, pressure increased from spans of 100 mm to 200 mm, and then remained nearly constant (with minor fluctuations) up to 400 mm. The peak pressure was identified at X = 0.03175 m. At the spoiler's leading edge, a

pronounced difference was observed between the upper and lower surface pressures, with a large pressure gap dominating the front region of the spoiler.

Analysis of the total deformations reveals that flexural deformation is the dominant type, rather than torsional deformation. This observation highlights the significance of bending forces in shaping the structural behavior and offers valuable insights into the response of the structure under external loads. The emphasis on flexural deformation underscores the need for design modifications and reinforces the importance of addressing bending moments to optimize the structural integrity and performance of the system (as depicted in Figure 6).

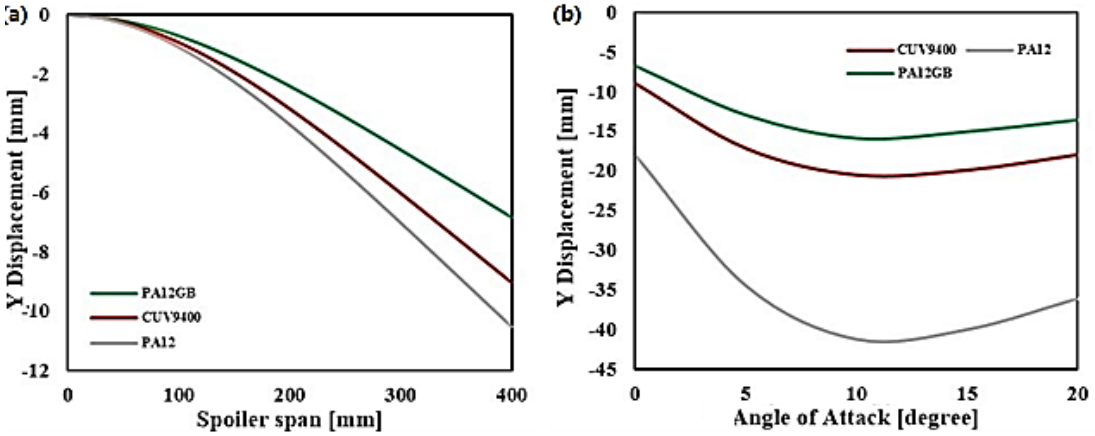

Figure 7. Spoiler at AOA 0° with 20 m/s flexional deformation (a) torsional deformation (b)

The analysis indicates that tip displacement increases with velocity up to the stall angle of attack, highlighting the influence of aerodynamic loads, which are dependent on geometry, flow conditions, and material properties. The cantilevered spoiler undergoes deformations along three axes (X, Y, Z), with Y-axis deformation being dominant, while X and Z deformations remain minimal. Maximum displacement occurs at the free end, farthest from the fixed support, as shown in red in Figure 7a. Flexural deformation exhibits a nonlinear distribution along the span. Near the clamped region (0–50 mm), deformations are small, while beyond 50 mm, deflections increase exponentially up to the spoiler tip at 400 mm (Figure 7a). Graphs of displacement versus angle of attack (AOA) demonstrate nonlinear growth in deformation with increasing AOA, reaching a peak at 11.5°, corresponding to the maximum downforce. Flexural deformation trends correlate with the material's Young's modulus; higher modulus materials display proportionally larger deformations. Across the velocity range of 10–30 m/s, the deformation pattern of Nylon and resin-based spoilers closely follows the downforce behavior.

Torsional deformation also exhibits a nonlinear response. In the first segment of the spoiler (clamped area to 41.67 mm), the twisting angle decreases to a minimum (−0.06893° to −0.10631° depending on the material). In the second segment (41.67–400 mm), the twisting angle increases to a maximum (0.1318° to 0.203°), as illustrated in Figure 7b. Flexural deformations increase until the stall region, after which they decrease. Material properties significantly affect the deformation patterns: the PA12 spoiler shows flexural deformation at stall nearly twice that of CUV9400 and 2.6 times that of PA12GB (Figure 8a). Torsional deformations also vary: PA12 exhibits substantial twisting, PA12GB shows modest torsion, and CUV9400 resin reaches a peak twist angle of 3° at 11° AOA, followed by a decline.

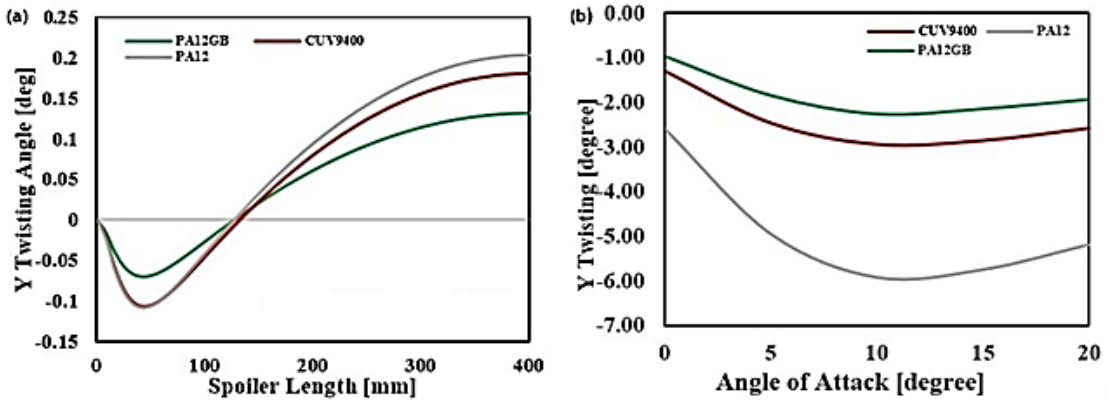

Figure 8. Spoiler deformation at 30 m/s (a) flexional deformation (b) torsional deformation

The torsional deformation of the spoiler exhibits a nonlinear pattern that is influenced by both material variations and changes in velocity, as shown in Figure 8b. Bending and torsional deformations exhibit parallel behavior; however, torsion occurs at a significantly smaller scale than bending. The high aspect ratio of the spoiler (4) and alignment of the aerodynamic axis, which closely coincide with the elastic axis, are the primary factors contributing to this distinction.

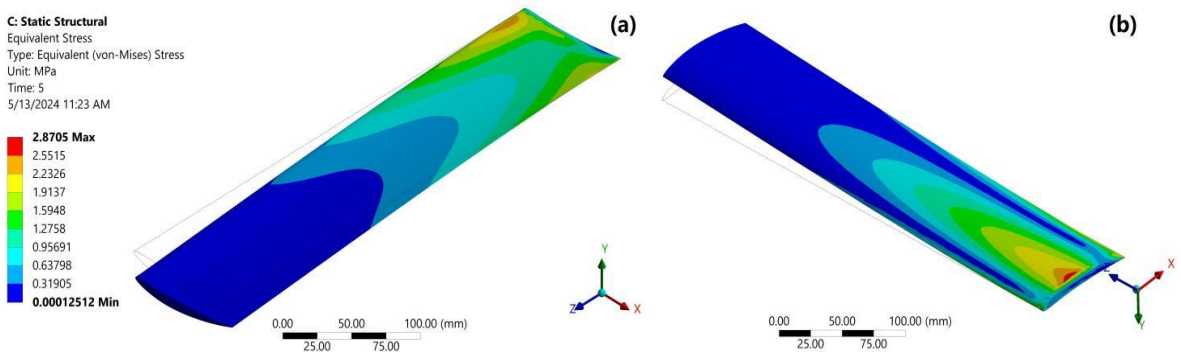

Figure 9. Equivalent von Mises stress of CUV9400 Spoiler at AOA 0° and 30 m/s (a) Top (b) Bottom

Torsional deformation is closely related to flexural deformation, although on a smaller scale, as illustrated in the twist per Angle of Attack (Twist/AOA) graph for various materials (Figure 9). The bending deformation exceeded the torsional deformation by a factor ranging from 50 to 68, depending on the specific values considered. This substantial difference indicates that bending is the predominant mode of deformation, whereas torsion becomes more prominent as the aspect ratio decreases.

Table 2. FEM equivalent stress (Von Mises)

Velocity [m/s]	Material	AOA [deg]	Max Equivalent Stress [MPa]
30	Nylon PA12	0	4.5995
		5	7.5667
		10	10.6650
		15	9.1079
		20	5.6403
	Resin CUV9400	0	4.6658
		5	7.8054
		10	10.9050
		15	9.2102
		20	5.7364
	Nylon PA12GB	0	4.7493
		5	7.8859
		10	11.0090
		15	9.3011
		20	5.8016

According to Von Mises theory, Equivalent Stress are recorded at speeds of 30 m/s and reach their maximum at an angle of attack of 10°, with values of 10.6 MPa for the PA12 spoiler, 10.9 MPa for the CUV9400, and 11 MPa for PA12GB spoilers (see Table 2). The trend of tensions follows that of deformations, increasing nonlinearly for angles of attack between 0 and 10°, and then decreasing for larger angles.

4. CONCLUSIONS

This study investigated the aerodynamic and structural behavior of a NACA 6409 airfoil section spoiler through a combination of numerical simulations and experimental analyses. The results revealed the nonlinear nature of aerodynamic loads, with the maximum equivalent von Mises stress observed as 10.6 MPa for Nylon PA12, 10.9 MPa for Resin CUV9400, and 11 MPa for Nylon PA12GB. The close agreement between numerical predictions and experimental measurements— < 6% for flexural deformations and 0–4.37% for torsional deformations—confirms the reliability of the FEA models within the spoiler's operational range.

Among the materials analyzed, PA12GB demonstrated the smallest overall deformations, making it the most suitable choice for minimizing structural deflection. The findings highlight the potential of 3D-printed plastic spoilers to achieve desired aeroelastic performance under various operating conditions. By adjusting the powder composition, spoilers with tailored flexural and torsional properties can be produced at low cost, suitable for different vehicle applications. This work emphasizes that high aspect ratio plastic spoilers, unlike aluminum or carbon fiber counterparts, exhibit more pronounced deformations. Quantifying these flexural and torsional responses provides critical insight into their design and material selection, paving the way for further development of cost-effective, high-performance spoilers.

ACKNOWLEDGEMENTS

The test was conducted in the Wind Tunnel at Wuhan University of Technology, and the numerical simulation was performed using ANSYS at the Slovak University of Technology.

FUNDING

This study was not supported by any grants from funding bodies in the public, private, or not-for-profit sectors.

CONFLICT OF INTEREST

The authors declare no conflicts of interest.

AUTHORS' CONTRIBUTION

Luigi Buffone (Conceptualisation, Supervision, Methodology, Validation, Formal analysis, Writing - original draft) Georgios Manganos (Investigation, Writing – review & editing)

Kavitha Mol S (Data curation, writing-review and editing)

All authors have read and agreed to the published version of the manuscript.

AVAILABILITY OF DATA AND MATERIALS

The datasets generated and/or analysed during the current study are available from the corresponding author on reasonable request.

ETHICS STATEMENT

This study did not involve human participants or animals. Ethical approval was therefore not required.

REFERENCES

[1] X. L. Wang, F. X. Wang, and Y. L. Li, "Aerodynamic characteristics of high-lift devices with downward deflection of spoiler," *Journal of Aircraft*, vol. 48, no. 2, pp. 730–735, 2011.

[2] M. S. Abood, I. Hussain, and A. H. Ali, "A theoretical and experimental investigation of the effects of inverted wings modifications on the stability and aerodynamic performance of a sedan car at cornering," *Engineering Reports*, vol. 7, no. 1, p. e13026, 2025.

[3] Z. Deng, S. Yu, W. Gao, Q. Yi, and W. Yu, "Review of effects the rear spoiler aerodynamic analysis on ground vehicle performance," *Journal of Physics: Conference Series*, vol. 1600, no. 1, p. 012027, 2020.

[4] G. Sivaraj, K. M. Parammasivam, and G. Suganya, "Reduction of aerodynamic drag force for reducing fuel consumption in road vehicle using basebleed," *Journal of Applied Fluid Mechanics*, vol. 11, no. 6, pp. 1489–1495, 2018.

[5] L. Buffone, G. Manganos, and Kavitha Mol S, "Experimental and Numerical Investigation of 3D-Printed Spoiler Deflection Under Cantilever Beam Conditions," *International Journal of Automotive and Mechanical Engineering*, vol. 22, no. 4, p. In Press, 2025.

[6] B. D. Lawrence, M. D. Coatney, F. Phillips, T. C. Henry, Y. Nikishkov, and A. Makeev, "Evaluation of the mechanical properties and performance cost of additively manufactured continuous glass and carbon fiber composites," *The International Journal of Advanced Manufacturing Technology*, vol. 120, no. 1, pp. 1135–1147, 2022.

[7] V. Chauhan, T. Kärki, and J. Varis, "Review of natural fiber-reinforced engineering plastic composites, their applications in the transportation sector and processing techniques," *Journal of Thermoplastic Composite Materials*, vol. 35, no. 8, pp. 1169–1209, 2022.

[8] S. R. Prabhu, M. Ilangkumaran, and T. Mohanraj, "3D printing of automobile spoilers using MCDM techniques," *Materials Testing*, vol. 62, no. 11, pp. 1121–1125, 2020.

[9] P. D. F. Teixeira and A. M. Awruch, "Numerical simulation of fluid–structure interaction using the finite element method," *Computers & Fluids*, vol. 34, no. 2, pp. 249–273, 2005.

[10] C. Antoci, M. Gallati, and S. Sibilla, "Numerical simulation of fluid–structure interaction by SPH," *Computers & Structures*, vol. 85, nos. 11–14, pp. 879–890, 2007.

[11] G. Alfonsi, "Reynolds-averaged Navier–Stokes equations for turbulence modeling," *Applied Mechanics Reviews*, vol. 62, no. 4, Art. no. 040802, 2009.

[12] G. Casalino, S. Polito, and L. Fabbiano, "Performance of SST k–ω turbulence model for aerodynamic flows," *Aerospace Science and Technology*, vol. 112, p. 106623, 2021.

[13] M. Abid, "Numerical simulation of external aerodynamic flows using SST k–ω turbulence model," *International Journal of Mechanical Engineering and Robotics Research*, vol. 14, no. 2, pp. 120–127, 2025.

[14] W. Krüger, I. Besselink, D. Cowling, D. B. Doan, W. Kortüm, and W. Krabacher, "Aircraft landing gear dynamics: Simulation and control," *Vehicle System Dynamics*, vol. 28, nos. 2–3, pp. 119–158, 1997.

[15] T. Hibiki and M. Ishii, "Lift force in bubbly flow systems," *Chemical Engineering Science*, vol. 62, no. 22, pp. 6457–6474, 2007.

[16] A. Bianchini, F. Balduzzi, G. Ferrara, and L. Ferrari, "Aerodynamics of Darrieus wind turbines airfoils: The impact of pitching moment," *Journal of Engineering for Gas Turbines and Power*, vol. 139, no. 4, p. 042602, 2017.

[17] W. Zhang and R. Samtaney, "Assessment of spanwise domain size effect on the transitional flow past an airfoil," *Computers & Fluids*, vol. 124, pp. 39–53, 2016.

[18] G. Ferrari, D. Federici, P. Schito, F. Inzoli, and R. Mereu, "CFD study of Savonius wind turbine: 3D model validation and parametric analysis," *Renewable Energy*, vol. 105, pp. 722–734, 2017.

[19] E. Sozer, C. Brehm, and C. C. Kiris, "Gradient calculation methods on arbitrary polyhedral unstructured meshes for cell-centered CFD solvers," in *Proc. 52nd Aerospace Sciences Meeting*, 2014, p. 1440.

[20] K. M. Almohammadi, D. B. Ingham, L. Ma, and M. Pourkashan, "Computational fluid dynamics (CFD) mesh independency techniques for a straight blade vertical axis wind turbine," *Energy*, vol. 58, pp. 483–493, 2013.

[21] F. J. Harewood and P. E. McHugh, "Investigation of finite element mesh independence in rate dependent materials," *Computational Materials Science*, vol. 37, no. 4, pp. 442–453, 2006.

[22] P. M. Knupp, "Achieving finite element mesh quality via optimization of the Jacobian matrix norm and associated quantities. Part I—A framework for surface mesh optimization," *International Journal for Numerical Methods in Engineering*, vol. 48, no. 3, pp. 401–420, 2000.

[23] T. Bein, H. Hanselka, and E. Breitbach, "An adaptive spoiler to control the transonic shock," *Smart Materials and Structures*, vol. 9, no. 2, pp. 141–150, 2000.

[24] F. Bastida, N. C. Bobillo-Ares, J. Aller, and N. C. Toimil, "Analysis of folding by superposition of strain patterns," *Journal of Structural Geology*, vol. 25, no. 7, pp. 1121–1139, 2003.

[25] L. Lanzoni and A. M. Tarantino, "The bending of beams in finite elasticity," *Journal of Elasticity*, vol. 139, no. 1, pp. 91–121, 2020.

[26] J. A. Maeck and G. De Roeck, "Dynamic bending and torsion stiffness derivation from modal curvatures and torsion rates," *Journal of Sound and Vibration*, vol. 225, no. 1, pp. 153–170, 1999.

[27] D. H. Chen, "Equivalent flexural and torsional rigidity of hexagonal honeycomb," *Composite Structures*, vol. 93, no. 7, pp. 1910–1917, 2011.

[28] S. Dong, R. S. Ponnuru, and R. A. Roberts, "Analysis of Euler–Bernoulli beams under combined loading," *Journal of Applied Mechanics*, vol. 67, no. 4, pp. 689–695, 2000.

[29] K. Olasek and P. Wiklak, "Application of 3D printing technology in aerodynamic study," *Journal of Physics: Conference Series*, vol. 530, no. 1, p. 012009, 2014.

[30] J. A. Wittkopf *et al.*, "3D printed electronics with multi jet fusion," in *Proc. NIP & Digital Fabrication Conference*, vol. 35, 2019, pp. 29–33.

[31] B. Msallem *et al.*, "Evaluation of the dimensional accuracy of 3D-printed anatomical mandibular models using FFF, SLA, SLS, MJ, and BJ printing technology," *Journal of Clinical Medicine*, vol. 9, no. 3, p. 817, 2020.

[32] B. Msallem *et al.*, "Dimensional accuracy in 3D printed medical models: A follow-up study on SLA and SLS technology," *Journal of Clinical Medicine*, vol. 13, no. 19, p. 5848, 2024.

[33] F. Fina *et al.*, "Fabricating 3D printed orally disintegrating printlets using selective laser sintering," *International Journal of Pharmaceutics*, vol. 541, nos. 1–2, pp. 101–107, 2018.

[34] O. D. Almeida, F. C. D. Miranda, O. Ferreira, and F. G. Saad, "Low subsonic wind tunnel—Design and construction," *Journal of Aerospace Technology and Management*, vol. 10, p. e1018, 2018.

[35] J. Moreno, R. Pérez, and A. Rodríguez, "Arduino-based data acquisition systems: A low-cost solution for experimental mechanics," *Measurement*, vol. 156, p. 107573, 2020.

[36] X. Jin, L. Wang, and H. Xu, "Smart data acquisition and signal processing for structural monitoring," *IEEE Transactions on Instrumentation and Measurement*, vol. 72, pp. 1–10, 2023.

[37] D. M. Ștefănescu, "Strain gauges and Wheatstone bridges—Basic instrumentation and new applications for electrical measurement of non-electrical quantities," in *Proc. Eighth International Multi-Conference on Systems, Signals & Devices*, 2011, pp. 1–5.

[38] J. Yang and Y. Lu, "Calibration of strain gauge sensors for structural health monitoring," *Sensors and Actuators A: Physical*, vol. 202, pp. 152–161, 2013.

[39] J. Beíndez, C. Rodríguez, and R. Alvarez, "Finite difference approaches for structural displacement analysis," *Applied Mathematical Modelling*, vol. 26, no. 9, pp. 803–817, 2002.

[40] T. Ohtsuki, "On the numerical determination of structural deflections under load," *Journal of Sound and Vibration*, vol. 329, no. 6, pp. 852–861, 2010.